



Timed Thermodynamic Process Model Applied to Submerged Arc Welding Modified by Aluminium-Assisted Metal Powder Alloying

THERESA COETSEE ^{1,2} and FREDERIK JOHANNES DE BRUIN ¹

1.—Department of Materials Science and Metallurgical Engineering, University of Pretoria, Pretoria 0002, South Africa. 2.—e-mail: theresa.coetsee@up.ac.za

An EERZ (effective equilibrium reaction zone) model was applied to the modified SAW (submerged arc welding) process to simulate the SAW process metallurgy in the gas-slag-metal reaction system. The SAW process was modified by adding Al as a de-oxidizer with alloying metal powders of Cr, Cu, and Ti. The static gas-slag-metal equilibrium model can accurately calculate the weld metal oxygen content (ppm O) for conventional SAW but not for the modified SAW process. The static equilibrium model overpredicts the reaction of Al. EERZ model runs were made for 2000–2500°C because this is the reported temperature range in the SAW arc cavity. The weld metal composition was adequately calculated, especially the weld metal ppm O, at the following effective equilibrium temperatures: 2400°C for Al-Cr additions, 2200°C for Al-Cr-Cu additions, and 2000°C for Al-Cr-Cu-Ti additions. Model results show that Ti metal powder can serve a de-oxidizer role in the presence of Al, resulting in Ti loss to the slag. Ti is also lost to the gas phase as $\text{TiF}_3(\text{g})$ and $\text{TiF}_2(\text{g})$ compared to little loss of Cr to the gas phase as $\text{Cr}(\text{g})$ and CrO to the slag phase.

INTRODUCTION

Effective modelling of element transfer behaviours in the submerged arc welding (SAW) process is a complex research topic. Much of the consumable development work, especially of fluxes, is based on empirically determined recipes. Therefore, developing fluxes is a tedious process based on much experimental work. In addition to flux design for physico-chemical properties such as viscosity, solidus and liquidus temperatures, and surface tension,

the first parameter in flux design is the weld metal ppm O. The latter parameter is most important because it sets the weld metal oxide inclusion content, which in turn sets adequate materials properties such as impact toughness and tensile strength. It has been established that weld metal ppm O should be 200 ppm O to 500 ppm O in carbon steel to ensure adequate materials properties. Some oxygen is required in the weld metal to form potent nucleation sites in the form of inclusions to form the desired acicular ferrite (AF) microstructure.^{1–3} The

$$\text{BI} = \frac{\% \text{CaF}_2 + \% \text{CaO} + \% \text{MgO} + \% \text{BaO} + \% \text{SrO} + \% \text{Na}_2\text{O} + \% \text{K}_2\text{O} + \% \text{Li}_2\text{O} + 0.5(\% \text{MnO} + \% \text{FeO})}{\% \text{SiO}_2 + 0.5(\% \text{Al}_2\text{O}_3 + \% \text{TiO}_2 + \% \text{ZrO}_2)} \quad (1)$$

empirical relationship of flux basicity index (Eq. 1) versus weld metal ppm O established by Tuliani et al.⁴ is widely used as a guideline in welding consumables specification.

Although this trend line is widely applicable, it cannot account for the addition of metallic alloying elements, especially de-oxidizer elements such as Si and Al. It has been clearly shown that the primary source of weld metal oxygen is the decomposition of oxides in the welding arc plasma with stability sequence from most to least stable measured as CaO, K₂O, Na₂O, TiO₂, Al₂O₃, MgO, SiO₂, and MnO.⁵ The addition of fluoride compounds, typically CaF₂, is used to dilute the flux oxide content to decrease the flux oxidation potential and limit hydrogen pick-up in the weld metal via water dissociation. Therefore, the flux forms an oxy-fluoride slag of complex reaction behaviours, including gas phase reactions.

In modelling the SAW metallurgy reactions, the approach has been to consider slag-metal equilibrium as a guideline, similar to de-oxidization equilibrium reactions in ladle metallurgy.^{6–8} Although it is accepted that the metallurgical reactions in the SAW process do not attain equilibrium, it is also well accepted that the reactions approach equilibrium and that slag-metal thermodynamic equilibrium expressions at least provide the reaction direction of element transfer between the slag and metal phases. The fast approach to reaction equilibrium is due to the rapid reaction kinetics at high reaction temperatures applied over small distances between phases of a high surface-to-volume ratio.^{6,9,10} The effective equilibrium temperature of reactions in the weld pool was calculated for 2000°C, which agrees with physical measurements.⁶ The arc cavity temperatures may vary from 2000°C to 2500°C.^{6,10} Therefore, SAW process modelling should cover these temperature values as input temperatures, especially when the gas phase is included. The slag-metal equilibrium modelling approach fits with the experimental work of Lau et al.¹¹ and Polar et al.¹² The authors measured the oxygen content of weld wire steel droplets at 2000 ppm O to 3000 ppm O. The weld wire steel droplets of high ppm O transfer their contained oxygen into the weld pool. Therefore, the high level of ppm O in the molten weld pool must be refined, and the formed oxide inclusions partially floated and absorbed into the molten flux (slag) to control the weld metal ppm O.¹³ The most extensive model for the SAW process metallurgy was developed by Mitra and Eagar.^{10,14,15} Their modelling approach

was to start with the trend line of Tuliani et al.⁴ as input and then calculate element transfer between the slag and weld pool metal by adding kinetic parameters and weld bead geometry parameters to the model. Thus, this work's important predictive capability of weld metal ppm O was missing. To the authors' knowledge, apart from the recently developed FactSage-based gas-slag-metal simulation model, no other models are available that can calculate the weld metal ppm O.¹⁶ The latter model was applied to conventional SAW without modification with metal powder additions as de-oxidizer or alloying elements. The authors modified the SAW process by adding Al powder as a de-oxidizer to enhance the element transfer behaviour of the easily oxidized metals of Cr and Ti. This paper aims to illustrate the need and benefit of applying a timed thermochemical model of the modified SAW process by applying the EERZ (effective equilibrium reaction zone) model to account for kinetic effects in gas-slag-metal reactions. FactSage 7.3 is used, similar to previously described models for ladle furnace (LF) and RH (Ruhrstahl Heraeus) process models.^{17,18} A similar model for Al-Ni-Cr-Co-Cu metal powder additions in SAW was applied in the authors' previous work.¹⁹

EXPERIMENTAL MATERIALS AND METHODS

The weld test results were reported in the authors' previous works. The base case (BC) weld test was done with conventional SAW.¹⁶ The MP2, MP4, and MP5 welding tests were made with Al powder as a de-oxidizer element and alloying metal powders, serving as the modified SAW process.^{20–22} All welds were made as bead-on-plate runs at the same welding heat input of 2.0 kJ/mm from welding parameters of 500 A, 28 V, and 42 cm/min welding speed at DCEP (direct current electrode positive). An aluminate basic agglomerated commercial flux of 0.2–1.6 mm particle size at a basicity index of 1.4 was applied in all welding tests. The chemical composition is shown in Table I. The flux chemistry was analysed by inductively coupled plasma optical emission spectroscopy (ICP-OES). The flux F-content was analysed using the titration method. The pure metal powders were sourced from Sigma-Aldrich (99.7% Al, – 1 mm), Alfa Aesar (99.0% Cr, – 44 μm), and Goodfellow (99.8% Cu, – 200 μm), PLS Technik GmbH & Co. (99.5% Ti, – 90 μm).

The base plate and weld wire compositions are summarized in Table II. The carbon steel plate, wire, and BC weld were analysed by optical

Table I. Flux composition

%MnO	%CaO	%SiO ₂	%Al ₂ O ₃	%CaF ₂	%MgO	%FeO	%TiO ₂	%Na ₂ O	%K ₂ O
7.0	0.1	20.6	25.9	18.1	23.2	2.2	1.0	1.7	0.2

Table II. Weld metal analyses

Test	ppm O	ppm N	%C	%Al	%Cr	%Cu	%Ti	%Si	%Mn	Balance
Plate	71	na	0.120	0.067	0.160	0.030	0.005	0.155	1.340	Fe
Wire	30	na	0.110	0	0	0.140	0	0.137	0.990	Fe
MP2	299	60	0.081	6.69	7.79	0.10	0.07	0.98	1.70	Fe
MP4	292	51	0.095	6.97	6.28	7.28	0.07	0.86	1.53	Fe
MP5	326	53	0.092	4.84	5.92	4.95	5.89	1.25	1.47	Fe
BC	499	na	0.110	0.03	0.11	0.11	0.01	0.26	1.30	Fe

Table III. Mass balance results

Test	Al (g)	Cr (g)	Cu (g)	Ti (g)	Total powder (g)	Wire (g)	Base plate (g)	Weld metal (g)	Slag (g)	Weld time (s)	%Weld metal above the plate
MP2	5.1	6.0	0	0	11.1	48.4	16.5	77	31.1	34.1	78
MP4	6.5	5.9	6.8	0	19.2	55.8	18.7	94	30.8	36.5	80
MP5	5.2	6.4	5.4	6.4	23.4	56.6	28.1	108	36.4	38.5	74
BC	0	0	0	0	0	67.5	67.5	135	65.9	48.9	50

emission spectroscopy (OES). The highly alloyed weld metals (MP2, MP4, MP5) were analysed by inductively coupled plasma optical emission spectroscopy (ICP-OES). Oxygen and nitrogen were analysed using the combustion method. The mass balance calculations for each weld run were used to determine the gram mass of each metal powder of Al, Cr, Cu, and Ti alloyed into the weld metal from adding 10 g of each metal powder element. The weld metal compositions and alloying powder mass balance values are summarized in Tables II and III. The post-weld slag mass and the added metal mass per weld run are summarized in Table III.

The model mass inputs were scaled to the mass balance measurements displayed in Table III. Because the mass of base metal, weld wire, slag, and each metal powder per total weld length and weld time was measured, the per-second mass of each reacting material is calculated from the numbers in Table III. The main assumptions in the mass balance are that the mass of slag equals the mass of flux that participated in the welding process, and only the quantity metal powders analysed in the weld metal are considered actively involved in the welding process.

SIMULATION MODEL

Motivation for EERZ Gas-Slag-Metal Model

The previous work applied the gas-slag-metal equilibrium model to model the conventional SAW process.^{16,23} An equilibrium temperature of 2100°C provided an adequate predictive calculation of the weld metal ppm O for different fluxes of varying basicity index.¹⁶ Figure 1 illustrates the better predictive capability of this model to the trend line

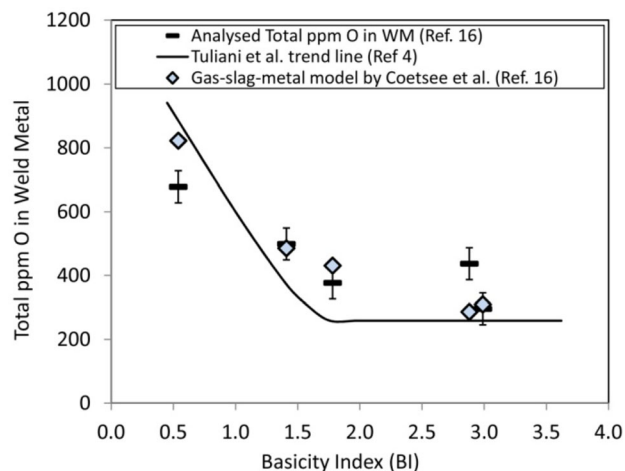


Fig. 1. Total ppm O in weld metal vs flux basicity index (BI): comparison of measured values from Ref. 16 versus Tuliani et al. trend line (Ref. 4) versus FactSage 7.3 gas-slag-metal model (Ref. 16). (This figure is reprinted from Ref. 24, under the terms of the Creative Commons CC BY license.).

of Tuliani et al.,⁴ especially at basicity values > 1.8. However, the application of this model to the modified SAW process with added metal powder does not calculate an adequately accurate weld metal composition.

This effect can be seen for the MP2 weld test from the values in Fig. 2a and b. The discrepancy between real weld metal composition values and calculated values is due to modification of the conventional SAW process by adding Al de-oxidizer and alloying metal powders. The values for 2200°C in Fig. 2a confirm that the model applied to conventional SAW results in an overestimation of

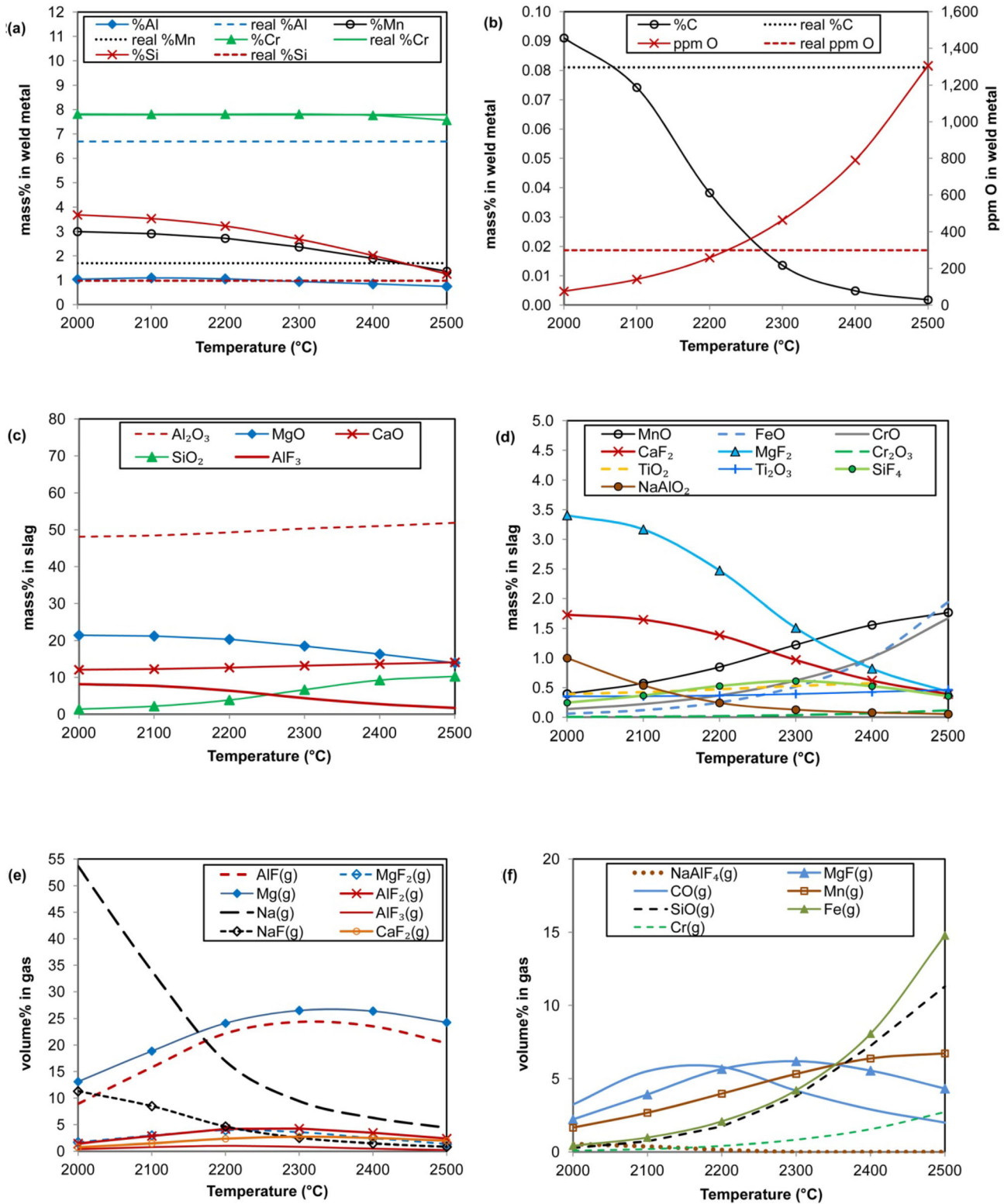


Fig. 2. MP2 phase compositions from gas-slag-metal equilibrium model.

Al reactions since the weld metal %Mn (2.7% versus 1.7%) and %Si (3.2% versus 0.98%) are over-predicted and the %Al (1.05% versus 6.7%) is under-predicted in the model, even though the calculated weld metal ppm O corresponds closely to the real

ppm O (258 ppm O versus 299 ppm O). Figure 2b shows that the weld metal ppm O varies widely with the input equilibrium temperature. At the temperature of 2100°C, which was used in the prior gas-slag-metal based model of conventional SAW, the

weld metal ppm O is calculated at 140 ppm O compared to the real value of 299 ppm O analysed in the weld metal (Table II). The %C in the weld metal is underpredicted for most equilibrium temperatures in Fig. 2b. Figure 2c and d shows the calculated slag analyses. The %Al₂O₃ is much higher than that of the flux in Table I, indicating oxidation of Al, which is in part due to aluminothermic reduction of MnO and SiO₂. Figure 2e and f shows the gas species calculated. Little Al-fluoride species is predicted in the slag phase since the Al-fluorides (AlF₃, AlF₂, AlF) are favoured to be in the gaseous state above 1200°C. The calculated gas compositions contain mostly AlF and Mg above 2200°C, whilst Na predominates below 2200°C. In conventional SAW, the weld slag FeO content correlates with the weld metal ppm O.^{14,16} This effect seen in the equilibrium calculations results as the ppm O in Fig. 2b, and the slag %FeO in Fig. 2f increases with increased temperature, thus representing an increased oxygen partial pressure in the gas-slag-metal system, from log P_{O₂} values of -11.6 at 2000°C to -7.0 at 2500°C. The apparent overprediction of the Al reaction extent in the gas-slag-metal equilibrium calculation indicates that mass-transfer effects should be included in the calculations. Therefore, an EERZ (effective equilibrium reaction zone) model approach was applied to set limits on the element transfer reactions per time step.^{17,18} This model was used in the authors' recent work on Al-Cr-Ni-Co-Cu metal powder alloying in SAW to illustrate the role of Al-gas reactions in the arc cavity.¹⁹

Model Inputs

The EERZ (effective equilibrium reaction zone) model contains reactor units representing the gas, slag, and metal phases. This modelling approach was applied to model steelmaking processes such as the ladle furnace (LF) and RH (Ruhrstahl Heraeus) decarburization process.^{17,18} The EERZ modelling method, as explained by Van Ende et al.,¹⁷ is based on the concept that all the phases within the "effective" reaction zone located next to the reaction interface are assumed to attain equilibrium. Therefore, equilibrium is not only attained at the reaction interface as is typical in diffusion control expressions. The EERZ modelling method uses an effective reaction volume instead of a mass-transfer coefficient value.¹⁷ High uncertainty in the input parameter values of the reaction areas, mass transfer coefficients, and boundary layer thickness at reaction interfaces motivate the application of the EERZ modelling method. This is especially so because the gas phase is included in calculations. Kinetic factor values represent the percentage of each phase reacting, as displayed in Fig. 3, introducing variable reaction extent for each phase in each time step. The following guideline was followed in scaling the kinetic factors, as displayed in Table IV. The kinetic

factor values for the slag and gas phases were scaled relative to those of the metal phase since the diffusivity values of the elements in liquid iron are known. The diffusivities of elements in liquid iron are in the range of 10⁻⁵-10⁻⁴ cm²/s.²⁵ Ionic diffusivities of Si⁴⁺ and O²⁻ in silicate slags are in the range of 4 × 10⁻⁷-1 × 10⁻⁶ cm²/s.²⁵ These data show that the metal phase diffusivity values are at least ten times those of the ions in silicate slag. This ratio was applied previously to scale the slag and metal kinetic factor values in an EERZ model for the LF.²⁶ Gas phase diffusivity coefficients are orders of magnitude larger than those of the metal phase at 10 cm²/s as a lower-end value.²⁷ The quantity of air input to the simulation was adjusted to attain the weld metal ppm value close to 60 ppm N, close to the analysed ppm N for the MP weld metals, as displayed in Table II. This air input quantity was maintained at the same value for all simulation runs at 1.4 × 10⁻⁷ kg/s. This is a small amount of air compared to the calculated gas evolution rate of 3.8 × 10⁻⁴ kg/s from the flux in the gas-slag-metal equilibrium calculation displayed in Fig. 2. The typical range of ppm N in SAW is 20-115 ppm N. The range for ppm N is much narrower than that of ppm O in the SAW weld metal at 200-1400.^{1,5,11} The main source of weld metal N in SAW is air, and the transfer pathway is via the metal droplets in the arc cavity, the same as for oxygen. The flux has little effect on N transfer in SAW, unlike the case for oxygen transfer, since the flux is a source of oxygen.^{5,11}

The model time intervals were scaled to the weld metal solidification time. The latter value was estimated at 3.5 s, as calculated from Christensen's equation, as explained by Klukan and Grong.¹³ Because the arc travels along the weld run, the welding process can be envisioned as forming and solidifying the weld pool in a series of weld metal solidification time steps. At the heat input of 2 kJ/mm applied in this work, the weld metal solidification time was calculated as 4 s. The total model time interval of 3 s was applied at half-second intervals, and the input masses of wire, metal powders, base plate, and flux were scaled to this time interval from the experimental measurements summarized in Table III. The kinetic factors for slag and metal were selected as increasing to a maximum value at the middle time steps and then decreasing because the heat input that drives the arc plasma, chemical, and melting reactions increases as the arc is positioned above the weld pool and then diminishes as the arc passes over the particular weld run position. The gas phase kinetic factor was kept at 100% since the gas phase diffusivity values are orders of magnitude larger than those of the metal and slag. The thermochemistry calculations are performed in the Equilib module of the FactSage 7.3 thermochemical software.²⁸ Macro script was used to iterate the equilibrium calculations in each reactor unit (R1 to R4) in Fig. 3 for each time step

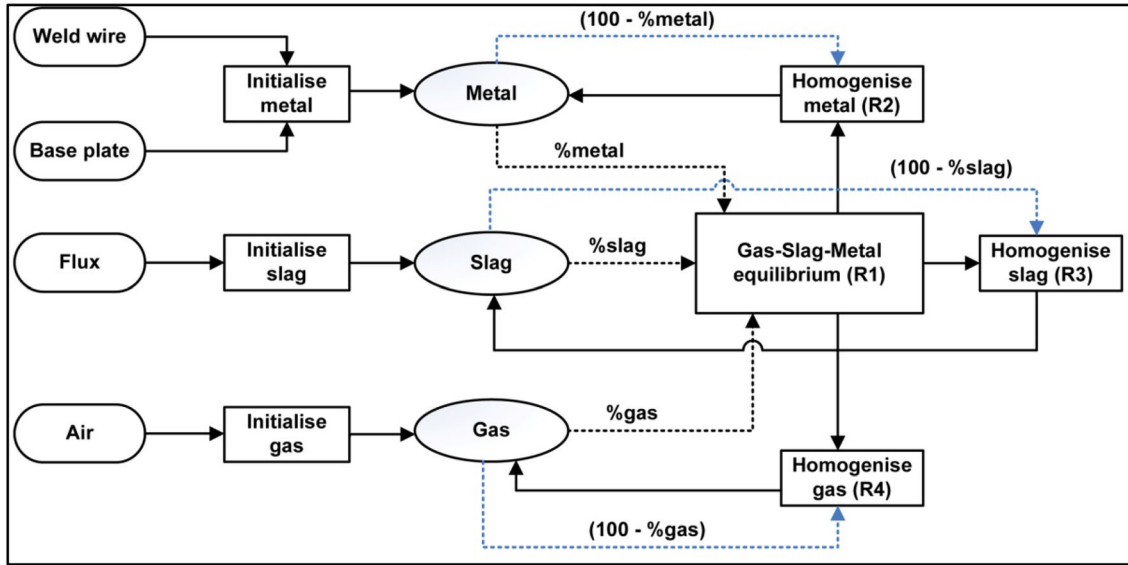


Fig. 3. Calculation flow diagram for EERZ model applied in SAW process simulation. (This figure is reprinted from Ref. 19, under the terms of the Creative Commons CC BY license.).

Table IV. Kinetic factors applied per time step

Time interval	1	2	3	4	5	6
%Metal stream reacting	10	20	60	60	40	20
%Slag stream reacting	1	2	6	6	4	2
%Gas stream reacting	100	100	100	100	100	100

and to interface with the spreadsheet-based input-output file. The FToxid, FSstel, and FactPS databases were included. The FToxid-SLAGA solution model was applied in all calculations. This solution model expresses the oxy-fluoride liquid slag composition in terms of oxide species mixed with the following fluoride species applicable to this work: NaF, KF, CaF₂, MgF₂, FeF₂, FeF₃, MnF₂, MnF₃, NiF₂, CuF, CrF₂, CrF₃, AlF₃, SiF₄, TiF₃, TiF₄, NaAlF₄, and KAlF₄.

Model Calculation Results and Discussion

The initial runs were made in the temperature range of 2000–2500°C, which corresponds to the high temperatures prevailing in the arc cavity.^{6,10} The results in Fig. 4 show the weld metal's end-point compositions as calculated in the EERZ model run at 2000–2500°C at 100°C intervals. The model can accurately calculate the weld metal ppm O. However, the temperature at which the weld metal ppm O is accurately calculated differs for each test scenario, namely 2400°C for MP2, 2200°C for MP4, and 2000°C for MP5. Interestingly, as seen in Fig. 4a, c, and d, the changes in the weld metal alloying elements are small for the different temperatures. The effective equilibrium temperature in the calculations decreased with increased metal

powder addition quantity. A possibility is that the amount of added metal powders had a net cooling effect in the weld pool since the required calculation equilibrium temperature seems to follow from high to low with low to high metal powder incorporation. Previously, the aluminothermic reduction reaction heat added to the weld pool was calculated to be similar for the weld tests at 97°C for MP2, 84°C for MP4, and 74°C.^{21,22} Therefore, variability in the aluminothermic reactions is probably not the reason for the differences in effective equilibrium calculation temperatures.

Figures 5, 6 and 7 display the composition versus time results from the EERZ model for each test scenario selected from the summarized end-point composition results in Fig. 4 to best match the weld metal ppm O using the same kinetic input factors as displayed in Table IV. In each scenario, the ppm O graph shows the values level off after 2 s, indicating the mass transfer effect in the calculation. The %C graph shows carbon loss due to oxidation, with the same mass transfer feature as ppm O, displayed in Figs. 5 and 6. In Fig. 7, the %C decrease is at a constant low rate. The product gas %CO ranged from 9.5% for MP2 to 5.9% for MP4, to 0.8% for MP5, which correlates to higher calculated carbon loss to 0.042 %C in MP2, 0.071 %C in MP4, and 0.089 %C in MP5.

In all three test scenarios, the weld metal chromium content remains stable, with little loss of Cr to the gas or slag phase. The de-oxidizer effect of Al is incorporated into the model and sufficiently dampened by the EERZ model method, as evidenced by the increase in Al₂O₃ in the slag in Figs. 5 and 6 accompanied by a decrease in %SiO₂ and the correspondence between the real and analysed weld metal %Al in Figs. 5, 6 and 7. Therefore, the EERZ

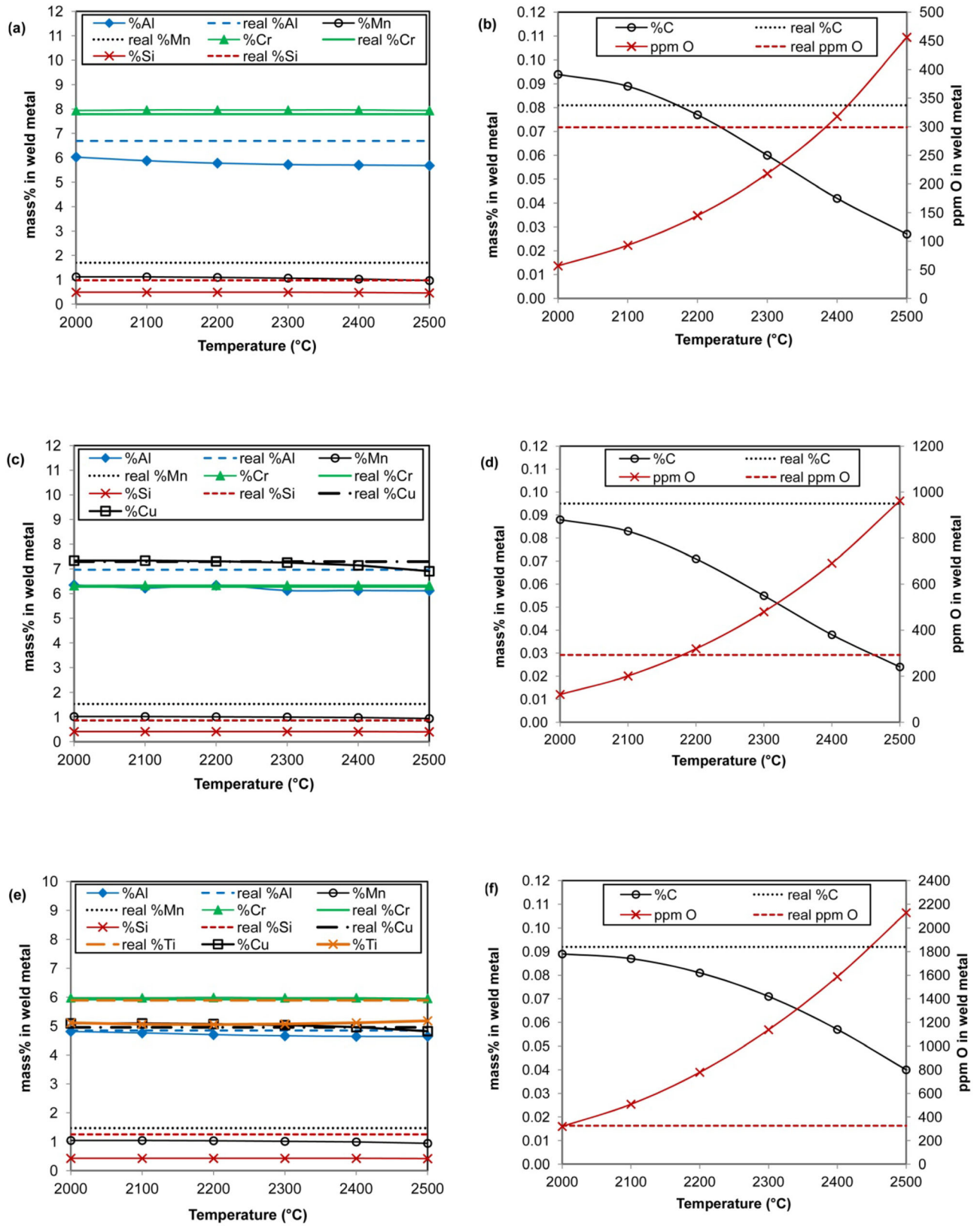


Fig. 4. End-point weld metal composition for temperatures of 2000–2500°C: MP2 = (a) and (b); MP4 = (c) and (d); MP5 = (e) and (f).

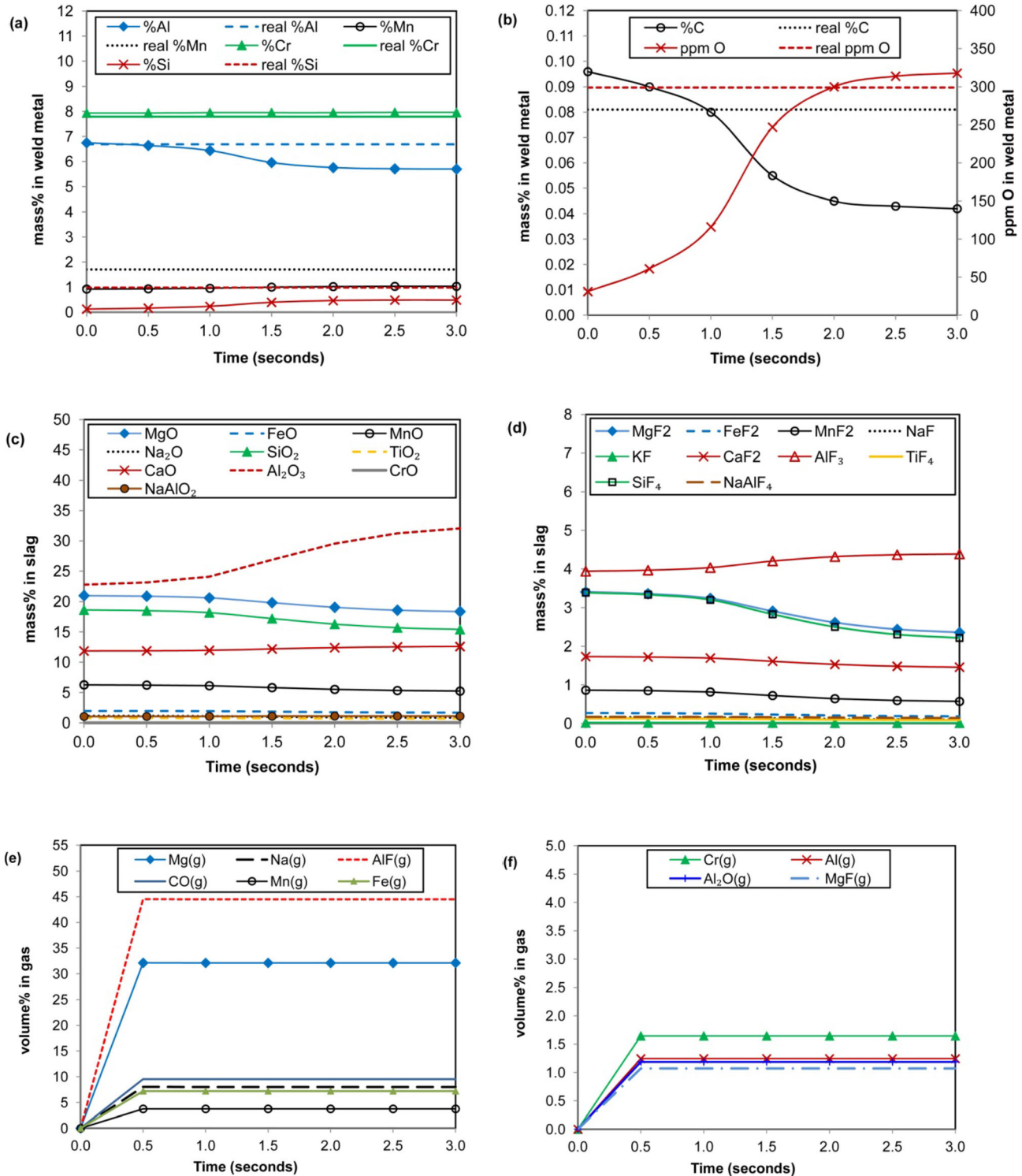


Fig. 5. Model calculation results for MP2 at 2400°C.

model can modulate the aluminothermic reactions to better calculate the end-point weld metal composition compared to the equilibrium model results in Fig. 2.

According to the model outputs in Fig. 7a and c, some of the Ti was oxidized to Ti₂O₃, even though

the expectation is that Al is a strong de-oxidizer and will limit Ti oxidation. Some of the Ti is also lost in the gas phase as TiF₃(g) and TiF₂(g), as displayed in Fig. 7e and f. The role of the added Al is to function as a total process de-oxidizer at the weld pool-slag interface and in the gas phase.¹⁹⁻²² The effect of Al

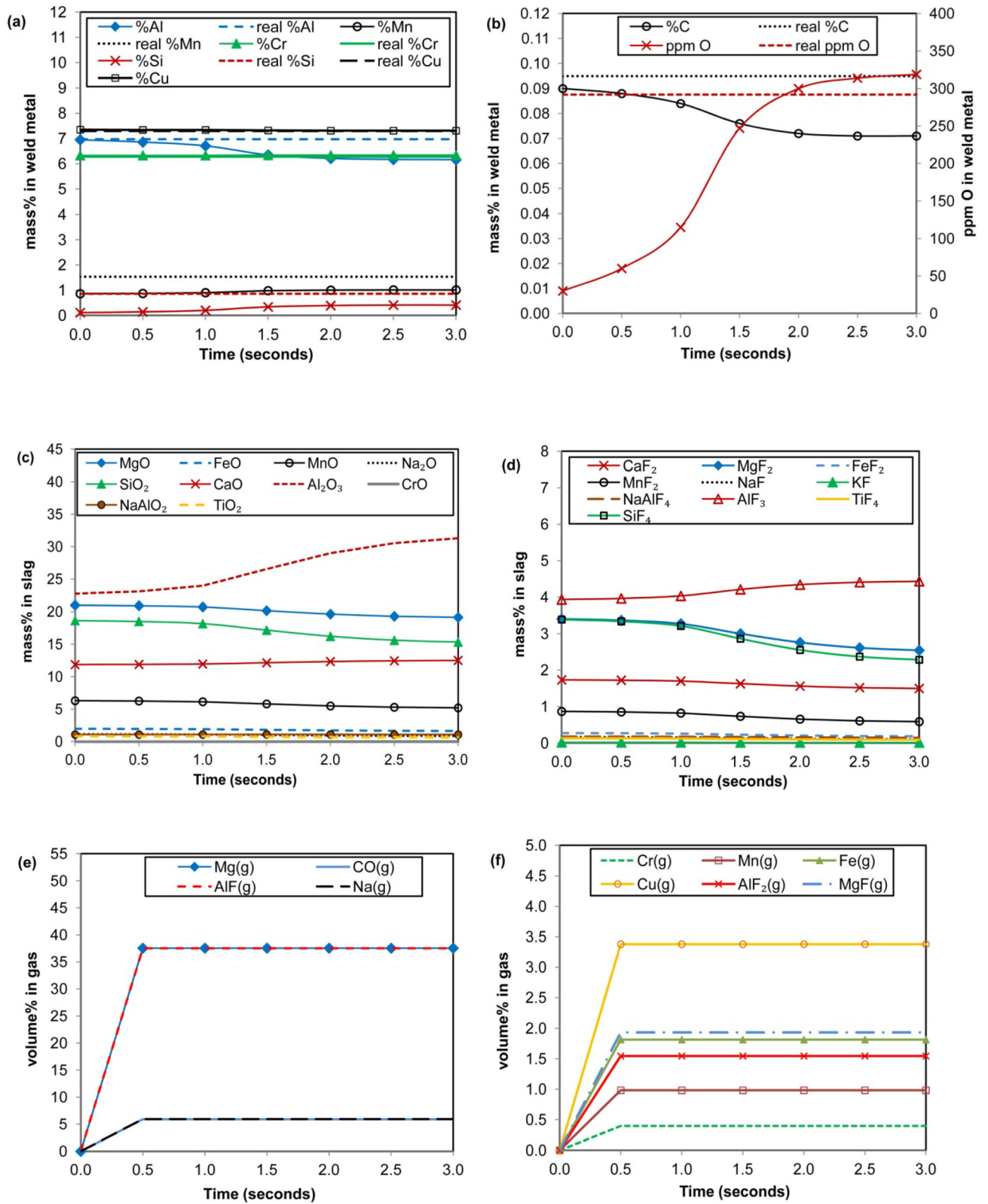


Fig. 6. Model calculation results for MP4 at 2200°C.

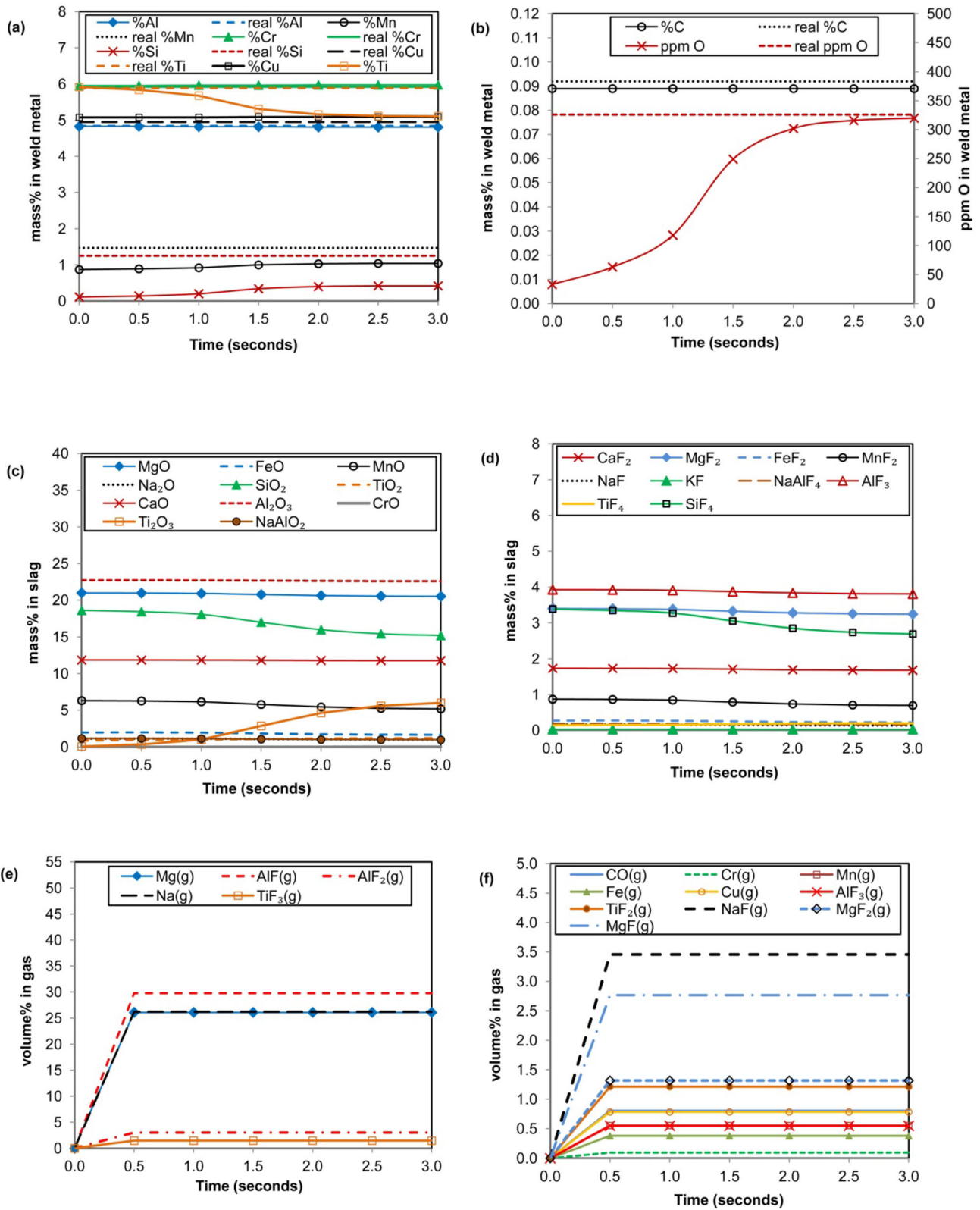
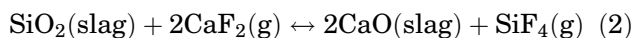


Fig. 7. Model calculation results for MP5 at 2000°C.

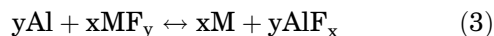
Table V. EERZ calculated partial oxygen pressure ($\log P_{O_2}$) versus $\log P_{O_2}$ at $[\%O]_{sat}$

Time interval	0	1	2	3	4	5	6	T (°C)	$[\%O]_{sat}$	$\log P_{O_2}$ at $[\%O]_{sat}$
MP2	-0.68	-8.9	-8.9	-8.9	-8.9	-8.9	-8.9	2400	2.39	-4.7
MP4	-0.68	-10.6	-10.6	-10.6	-10.6	-10.6	-10.6	2200	1.53	-5.3
MP5	-0.68	-12.6	-12.6	-13.6	-12.6	-12.6	-12.6	2000	0.91	-6.1
BC	-0.68	-8.1	-8.1	-8.1	-8.1	-8.1	-8.1	2150	1.35	-5.5

on the formation of gas phase species is clear, as $AlF(g)$, $Mg(g)$, and $Na(g)$ are the major gas species. With decreased temperature, the calculated Al-gas species shift from $Al(g)$, $AlF(g)$, and $Al_2O(g)$ at $2400^\circ C$ to $Al(g)$, $AlF(g)$, and $AlF_2(g)$ at $2200^\circ C$ to $Al(g)$, $AlF(g)$, $AlF_2(g)$, and $AlF_3(g)$ at $2000^\circ C$. In comparison, simulation results for conventional SAW with the same flux, the base case (BC), calculated for $2100^\circ C$, indicated the main gas species as MgF_2 , AlF_3 , NaF , CaF_2 , CO , $NaAlF_4$, Na , AlF_2 , MgF , TiF_3 , $KAlF_4$, and minor species as K , KF , Mg , AlF , Mn , Fe , SiF_4 , and SiO at less than 1 vol% concentration. In SAW literature, the primary reaction often cited to explain the transformation of CaF_2 is reaction 2.⁵ In the same way, the other oxides in the slag may transform into gas species; for example, $KF(g)$ and $NaF(g)$ formed from reaction of K_2O and Na_2O in the slag. Alumina may also be transformed into the gas phase via reaction 2 to form Al-fluorides.²⁹



The addition of Al as de-oxidizer shifts the gas phase species to Al-fluorides and elemental gasses such as $Mg(g)$ and $Na(g)$ with less $CaF_2(g)$, $MgF_2(g)$, and $CO(g)$ as seen in the base case (BC) product gas. The displacement of the fluorides by Al via reaction 3 is thermodynamically favoured.^{19,24} Therefore, in addition to the de-oxidizer role of Al to prevent loss of alloying elements to the slag via oxidation, the role of Al is also to form Al-fluorides in the gas instead of less stable metal fluorides to release the metal vapour into the arc cavity via reaction 3.



Figures 5, 6 and 7 show that the gas phase contains small percentages of metallic vapour of Fe, Mn, Cr, and Cu. The role of Al de-oxidizer is to prevent oxidation loss of easily oxidizable elements such as Cr and Ti. The formation of Ti-fluoride gasses and Ti_2O_3 in the slag indicates that the loss of Ti is limited but not excluded. The less readily formed Cr-fluoride gasses and lesser affinity of Cr for oxygen means that the limited Cr loss occurs in metallic Cr vapour only compared to Ti loss to the gas and slag phases.

The partial oxygen pressure values from the EERZ model for MP2, MP4, and MP5 are summarized in Table V compared with the EERZ model run for the base case. In all instances, the initial gas

composition is air. Within the first second, the gas phase composition is dramatically changed, as shown in Figs. 5, 6 and 7, and the oxygen partial pressure in the gas phase is significantly lowered. The solubility of oxygen in pure liquid iron in equilibrium with pure liquid iron oxide is shown in Table V with its equivalent $\log P_{O_2}$ values as calculated from literature-reported equations.³⁰ These values show that a lower effective equilibrium temperature accords with more reducing conditions in terms of thermodynamics. Despite the effect of temperature on oxygen solubility, the comparison of $\log P_{O_2}$ values with and without Al de-oxidiser addition shows the lowering effect of Al additions in the gas phase oxygen partial pressure, which in turn induces a lower oxygen partial pressure at the slag-weld pool interface.

The delta values in the weld metal composition are summarized in Table VI. Although the calculated weld metal values of %C, %Mn, and %Si are underpredicted, these values are closer than the values calculated in the static gas-slag-metal equilibrium model. More importantly, the Al reactions are better weighted in the model, in contrast to the static gas-slag-metal equilibrium model which calculated most of the Al as oxide in the slag. It may be possible to improve the model accuracy by adjusting the kinetic factors. However, the uncertainty in the selected equilibrium temperatures is the most important factor in setting model accuracy because temperature sets the weld metal ppm O first, and the rest of the output parameters appear secondary. Accurate weld metal ppm O from a model calculation is the most important output required for a useful SAW model.

Therefore, the EERZ model method provides more detailed insights into the modified SAW process with Al added as the de-oxidizer element. Although gas phase composition measurements in the extreme conditions of the arc cavity have been done, it is a complicated procedure.³¹ The model approach can provide guidelines and so limit the physical work quantity required to develop new flux formulations.

CONCLUSION

An EERZ (effective equilibrium reaction zone) model based on gas-slag-metal equilibrium was developed to simulate the modified SAW process with added metal powders. This model can simulate

Table VI. Delta values in weld metal composition (model value-real analysed value)

	%C	%Mn	%Si	%Al	%Cr	%Cu	%Ti
MP2 (g-s-m)	- 0.043	1.02	2.25	- 5.64	0.03	-	-
MP2	- 0.039	- 0.67	- 0.50	- 0.99	0.17	-	-
MP4	- 0.024	- 0.52	- 0.45	- 0.81	0.06	0.01	-
MP5	- 0.003	- 0.43	- 0.83	- 0.03	0.06	0.14	- 0.78

the modified SAW process to calculate the weld metal composition for 2000–2400°C for added Al powder as a de-oxidizer with Cr, Ti, and Cu alloying metal additions. The most crucial simulation calculation requirement is to calculate the weld metal ppm O to realistic values because flux formulations are specified with regard to flux basicity to attain a target weld metal ppm O, which in turn sets the quantity of oxide inclusions in the weld metal that sets the weld metal materials properties. The simulation results indicate that the effective equilibrium temperature varies for the different test scenarios of alloy additions. The de-oxidizer effect of Al was effectively captured in the model. The model calculations show that the added Ti metal powder can also serve a de-oxidizer role in the presence of Al, resulting in Ti loss to the slag.

FUNDING

Open access funding provided by University of Pretoria.

CONFLICT OF INTEREST

On behalf of all authors, the corresponding author states that there is no conflict of interest.

OPEN ACCESS

This article is licensed under a Creative Commons Attribution 4.0 International License, which permits use, sharing, adaptation, distribution and reproduction in any medium or format, as long as you give appropriate credit to the original author(s) and the source, provide a link to the Creative Commons licence, and indicate if changes were made. The images or other third party material in this article are included in the article's Creative Commons licence, unless indicated otherwise in a credit line to the material. If material is not included in the article's Creative Commons licence and your intended use is not permitted by statutory regulation or exceeds the permitted use, you will need to obtain permission directly from the copyright holder. To view a copy of this licence, visit <http://creativecommons.org/licenses/by/4.0/>.

REFERENCES

1. C.B. Dallam, S. Liu, and D.L. Olson, *Weld. J.* 64, 140 (1985).
2. T. Koseki and G. Thewlis, *Mat. Sci. Technol.* 21, 867 <http://doi.org/10.1179/174328405X51703> (2005).
3. D.S. Sarma, A.V. Karasev, and P.G. Jönsson, *ISIJ Int.* 49, 1063 <https://doi.org/10.2355/isijinternational.49.1063> (2009).
4. S.S. Tuliani, T. Boniszewski, and N.F. Eaton, *Weld. Met. Fabr.* 37, 327 (1969).
5. C.S. Chai and T.W. Eagar, *Weld. J.* 61, 229 (1982).
6. C.S. Chai and T.W. Eagar, *Metall. Trans. B* 12, 539 <https://doi.org/10.1007/bf02654325> (1981).
7. J.H. Palm, *Weld. J.* 51, 358 (1972).
8. U. Mitra and T.W. Eagar, *Metall. Trans. A* 15, 217 <https://doi.org/10.1007/bf02644404> (1984).
9. J.E. Indacochea, M. Blander, N. Christensen, and D.L. Olson, *Metall. Trans. B* 16, 237 <https://doi.org/10.1007/BF02679715> (1985).
10. U. Mitra and T.W. Eagar, *Metall. Trans. B* 22, 65 <https://doi.org/10.1007/bf02672528> (1991).
11. T. Lau, G.C. Weatherly, and A. McLean, *Weld. J.* 64, 343 (1985).
12. A. Polar, J.E. Indacochea, and M. Blander, *Weld. J.* 69, 68 (1990).
13. A.O. Kluken and Ø. Grong, *Metall. Trans. A* 20, 1335 <http://doi.org/10.1007/BF02665492> (1989).
14. U. Mitra and T.W. Eagar, *Metall. Trans. B* 22, 73 <https://doi.org/10.1007/bf02672529> (1991).
15. U. Mitra and T.W. Eagar, *Metall. Trans. B* 22, 83 <https://doi.org/10.1007/bf02672530> (1991).
16. T. Coetsee, R.J. Mostert, P.G.H. Pistorius, and P.C. Pistorius, *J. Mater. Res. Technol.* 11, 2021 <https://doi.org/10.1016/j.jmrt.2021.02.046> (2021).
17. M.-A. Van Ende, Y.-M. Kim, M.-K. Cho, and I.-H. Jung, *Metall. Trans. B* 42, 477 <https://doi.org/10.1007/s11663-011-9495-4> (2011).
18. S.P. Piva, D. Kumar, and P.C. Pistorius, *Metall. Trans. B* 48, 37 <https://doi.org/10.1007/s11663-016-0764-0> (2017).
19. T. Coetsee and F. De Bruin, *Processes* 11, 2110 <https://doi.org/10.3390/pr11072110> (2023).
20. T. Coetsee and F. De Bruin, *High Temp. Mater. Process.* 40, 421 <https://doi.org/10.1515/htmp-2021-0051> (2021).
21. T. Coetsee and F. De Bruin, *Processes* 10, 296 <https://doi.org/10.3390/pr10020296> (2022).
22. T. Coetsee and F. De Bruin, *Processes* 10, 452 <https://doi.org/10.3390/pr10030452> (2022).
23. J. Zhang, T. Coetsee, S. Basu, and C. Wang, *Calphad* 71, 102195 <https://doi.org/10.1016/j.calphad.2020.102195> (2020).
24. T. Coetsee and F. De Bruin, *Processes* 10, 658 <https://doi.org/10.3390/pr11030658> (2023).
25. E.T. Turkdogan, *Fundamentals of Steelmaking* (The Institute of Materials, Cambridge, 1996), pp176–177.
26. D. You, S.K. Michelic, and C. Bernhard, *Steel Res. Int.* 91, 2000045 <https://doi.org/10.1002/srin.202000045> (2020).
27. D.R. Poirier and G.H. Geiger, *Transport Phenomena in Materials Processing* (TMS, Warrendale, 1994), pp453–456.

28. C.W. Bale, E. Béglise, P. Chartrand, S. Deckerov, G. Eriksson, A.E. Gheribi, K. Hack, I.-H. Jung, Y.-B. Kang, J. Melançon, et al., *Calphad* 55, 1 <https://doi.org/10.1016/j.calphad.2016.07.004> (2016).
29. T. Lau, G.C. Weatherly, and A. McLean, *Weld. J.* 65, 31 (1986).
30. E.T. Turkdogan, *Fundamentals of Steelmaking* (The Institute of Materials, Cambridge, 1996), pp112–113.
31. G. Gött, A. Gericke, K.M. Henkel, and D. Uhrlandt, *Weld. J.* 95, 491 (2016).

Publisher's Note Springer Nature remains neutral with regard to jurisdictional claims in published maps and institutional affiliations.